

# *Ab initio* downfolding based on the GW approximation for infinite-layer nickelates

Motoaki Hirayama<sup>1,2\*</sup>, Yusuke Nomura<sup>2</sup>, Ryotaro Arita<sup>2,3</sup>

<sup>1</sup> QPEC, The University of Tokyo, Hongo, Tokyo, 113-8656, Japan

<sup>2</sup> RIKEN Center for Emergent Matter Sciences (CEMS), Wako, Saitama, 351-0198, Japan

<sup>3</sup> Department of Applied Physics, The University of Tokyo, Hongo, Tokyo, 113-8656, Japan

Correspondence\*:

Motoaki Hirayama

hirayama@ap.t.u-tokyo.ac.jp

## ABSTRACT

We derive an effective three-orbital model for the infinite-layer nickelates based on the band structure obtained by the GW approximation (GWA), where we consider the Ni  $3d_{x^2-y^2}$  and O  $2p$  orbitals forming the  $\sigma$ -bond. In the GWA, the self-energy correction to the local density approximation (LDA) increases the energy difference between Ni  $3d_{x^2-y^2}$  and O  $2p$ , which reduces the bandwidth of the antibonding  $3d_{x^2-y^2}$  orbitals. The isolation of the Ni  $3d_{x^2-y^2}$  around the Fermi level suppresses the screening effect. As a result, the correlation effect becomes more significant than that in the model constructed by the LDA-based downfolding. Furthermore, the Mott-Hubbard type character is enhanced in the GWA-based effective model, because the charge-transfer energy increases more rapidly compared to the increase in the interaction parameters.

**Keywords:** nickelate superconductivity, density functional theory, GW approximation, *ab initio* downfolding

## 1 INTRODUCTION

The discovery of nickel superconductors [1] has attracted renewed attention to superconductivity in strongly correlated electron systems [2, 3, 4, 5, 6, 7]. So far, superconductivity has been found in film samples of doped infinite-layer nickelates  $R\text{NiO}_2$  ( $R=\text{Nd, Pr, and La}$ ) [1, 8, 9, 10, 11, 12, 13, 14, 15, 16] and a quintuple-layer nickelate  $\text{Nd}_6\text{Ni}_5\text{O}_{12}$  [17]. Although the nature of the superconductivity is largely unknown, the pairing mechanism is likely to be unconventional: Theoretically, a phonon calculation for  $\text{NdNiO}_2$  has shown that the electron-phonon coupling is too weak to explain the superconductivity with a transition temperature on the order of 10 K [18]. Experimentally, both  $U$ - and  $V$ -shaped spectra have been observed using the scanning tunneling microscopy, depending on the location of the inhomogeneous surface of the doped  $\text{NdNiO}_2$  film [9]. Although the origin of the coexistence of the two different signals is controversial [19, 20, 21, 22, 23], the presence of the  $V$ -shape spectrum is consistent with an unconventional  $d$ -wave pairing. In fact, unconventional pairing mechanisms have been discussed since the early stages of the research [24, 25, 26].

In contrast with the conventional phonon-mediated superconductivity for which *ab initio* calculation based on density functional theory (DFT) plays a crucial role [27, 28], construction of low-energy models with few degrees of freedom is critically important for unconventional superconductivity since a detailed analysis of the correlation effects is mandatory. In the standard approach to derive a low-energy effective

model from first principles, we first calculate the electronic structure with the local density approximation (LDA) or the generalized gradient approximation (GGA) in the framework of DFT. We then construct the maximally localized Wannier function (MLWF) [29, 30] for the low-energy states around the Fermi level and derive a tight-binding model. Next, we calculate the effective Coulomb interaction by the constrained random phase approximation (cRPA) [31, 32]. The matrix elements of the (partially) screened interaction are calculated for the Wannier basis, from which we estimate the Hubbard  $U$  and Hund coupling  $J$  in the multi-orbital Hubbard model [18, 24, 33, 34]. The cRPA is formulated in such a way that RPA calculation for the derived low-energy effective model reproduces a one-shot GW ( $G_0W_0$ ) result [31, 32, 35].

To improve the accuracy of the parameters in the low-energy model, we can replace the Green's function ( $G_0$ ) constructed from the DFT/LDA eigenenergies with the dressed Green's function in the GW approximation (GWA)<sup>1</sup>. Such a derivation based on the GWA has been recently performed for the celebrated cuprate superconductors [37, 38]. While two types of orbitals, i.e., the Cu  $3d$  and O  $2p$  orbitals, form low-energy bands near the Fermi level, the GW self-energy correction increases the energy difference between the  $d$  and  $p$  orbitals and reduce the bandwidth of the  $d$  band. With these modifications, it has been shown with an extensive variational Monte Carlo (VMC) calculation that the experimental values of the Mott gap and magnetic moment of  $\text{La}_2\text{CuO}_4$  are successfully reproduced [38, 39]. Given that the differences in the band structure between the DFT/LDA and that in the GWA are commonly seen in transition metal oxides where  $3d$  and  $2p$  orbitals with different correlation strengths coexist near the Fermi level, it would be of great interest to derive an effective low-energy model for infinite-layer nickelates based on the GWA.

In this study, we perform a first-principles derivation of the effective model for infinite-layer nickelates. In particular, we mainly focus on the  $dpp$  three-orbital models (single-orbital model is discussed in Appendix) because it is interesting to investigate how the GWA modifies the charge-transfer energy and correlation strength compared to the LDA-based downfolding.<sup>2</sup> First, we calculate the band structure in the DFT/LDA and estimate the parameter of the effective model using the MLWF and cRPA technique. Next, we calculate the band structure in the GWA using the Green's function of the LDA. We derive the effective model from the GW band structure and compare the results with those obtained from the LDA. We find that the GWA-based effective model is predicted to be more strongly-correlated with enhanced Mott-Hubbard type character. The model offers an interesting reference to be compared with that of the cuprates with the charge-transfer type character.

<sup>1</sup> It should be noted that although the cRPA method is free from the double counting problem for the interaction parameters, we have to apply the constrained GW (cGW) method to avoid the double counting in the self-energy [36].

<sup>2</sup> We note that there are several other effective models for infinite-layer nickelates that have been discussed, including a multi-band model that includes  $3d$  orbitals other than the  $3d_{x^2-y^2}$  orbital [40, 41, 42, 43, 44, 45, 46, 47, 48, 49, 50, 51, 52], a model that includes the contribution of rare-earth  $4f$  electrons [53, 54, 55, 56], and a model that includes the self-doping bands [57, 58, 59]. Here, we focus on the debate [57, 60, 61, 40, 62, 63, 64, 65, 66, 67] on the classification of the Mott-Hubbard or charge-transfer regimes in Zaanen-Sawatzky-Allen phase diagram [68].

## 2 METHOD

In this study, we calculate the parameter of the Hubbard Hamiltonian for the low-energy degree of freedom,

$$\begin{aligned} \mathcal{H}^{\text{eff}} = & \sum_{ij} \sum_{\ell_1 \ell_2 \sigma} t_{\ell_1 \ell_2 \sigma}(\mathbf{R}_i - \mathbf{R}_j) d_{i\ell_1 \sigma}^\dagger d_{j\ell_2 \sigma} \\ & + \frac{1}{2} \sum_{i_1 i_2 i_3 i_4} \sum_{\ell_1 \ell_2 \ell_3 \ell_4 \sigma \eta \rho \tau} \left\{ W_{\ell_1 \ell_2 \ell_3 \ell_4 \sigma \eta \rho \tau}^{\text{H}}(\mathbf{R}_{i_1}, \mathbf{R}_{i_2}, \mathbf{R}_{i_3}, \mathbf{R}_{i_4}) \right. \\ & \left. d_{i_1 \ell_1 \sigma}^\dagger d_{i_2 \ell_2 \eta} d_{i_3 \ell_3 \rho}^\dagger d_{i_4 \ell_4 \tau} \right\}. \end{aligned} \quad (1)$$

Here, the hopping term is represented by

$$t_{\ell_1 \ell_2 \sigma}(\mathbf{R}) = \langle \phi_{\ell_1 \mathbf{0}} | H | \phi_{\ell_2 \mathbf{R}} \rangle, \quad (2)$$

where  $H$  is the Hamiltonian in the LDA or GWA and  $\phi_{\ell \mathbf{R}}$  is the MLWF of the  $\ell$ th orbital localized at the unit cell  $\mathbf{R}$ . The interaction term is given by

$$W_{\ell_1 \ell_2 \ell_3 \ell_4 \sigma \eta \rho \tau}^{\text{H}}(\mathbf{R}_{i_1}, \mathbf{R}_{i_2}, \mathbf{R}_{i_3}, \mathbf{R}_{i_4}) = \langle \phi_{\ell_1 \mathbf{R}_{i_1}} \phi_{\ell_2 \mathbf{R}_{i_2}} | W^{\text{H}} | \phi_{\ell_3 \mathbf{R}_{i_3}} \phi_{\ell_4 \mathbf{R}_{i_4}} \rangle, \quad (3)$$

where  $W^{\text{H}}$  is the effective interaction for the low-energy degree of freedom,

$$W^{\text{H}}(q, \omega) = \frac{v(q)}{1 - P^{\text{H}}(q, \omega)v(q)}. \quad (4)$$

We calculate the effective interaction from the one-shot GWA band. In the one-shot GWA, we calculate the self-energy from the Green's function  $G$  and the fully-screened interaction  $W$ ,

$$\Sigma = GW, \quad (5)$$

where  $W$  is calculated from all the polarizations in the RPA  $P$  as follows,

$$W(q, \omega) = \frac{v(q)}{1 - P(q, \omega)v(q)}. \quad (6)$$

The quasiparticle approximation of the Hamiltonian in the GWA is expressed as

$$H^{\text{GW}} = H^{\text{LDA}} + Z(\epsilon^{\text{LDA}})(-V^{\text{xc}} + \Sigma(\epsilon^{\text{LDA}})), \quad (7)$$

where  $H^{\text{LDA}}$  is the Hamiltonian in the LDA,  $V^{\text{xc}}$  is the exchange correlation potential in the LDA, and  $Z(\epsilon^{\text{LDA}})$  is the renormalization factor of  $\Sigma$  at the eigenenergy  $\epsilon^{\text{LDA}}$ :

$$Z(\epsilon) = \left\{ 1 - \frac{\partial \text{Re} \Sigma}{\partial \omega} \Big|_{\omega=\epsilon} \right\}^{-1}. \quad (8)$$

We calculate the electronic band structure of the YNiO<sub>2</sub> using the experimental lattice parameters of LaNiO<sub>2</sub>, where  $a = 3.959 \text{ \AA}$  and  $c = 3.375 \text{ \AA}$  [69]. To exclude the contribution of the  $4f$  orbital, here

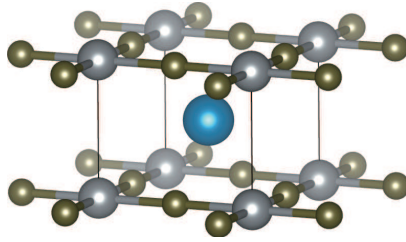


**Figure 1.** Crystal structure of  $\text{YNiO}_2$ .

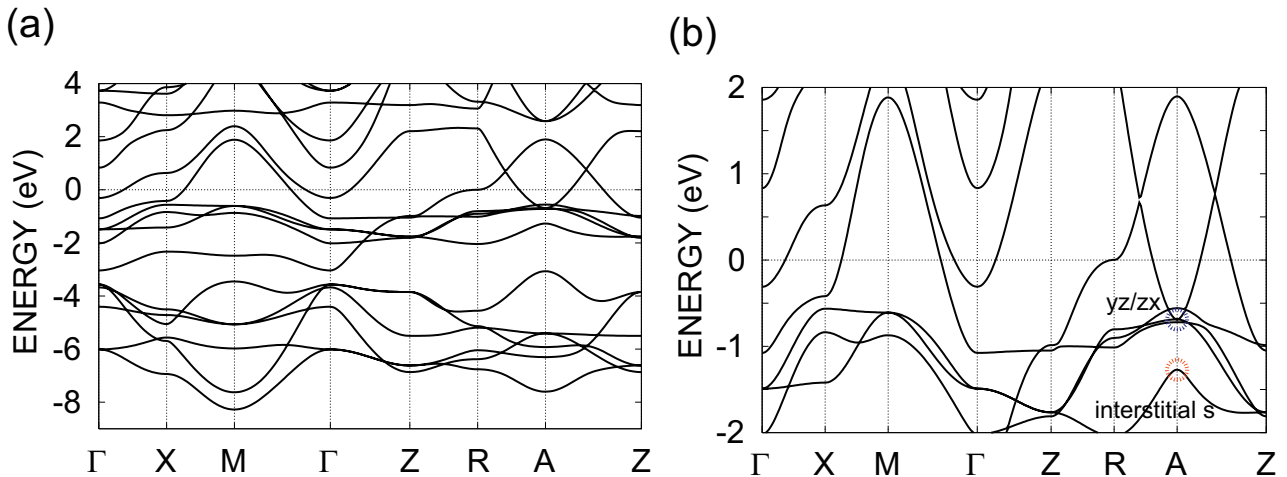


**Figure 2.** (a) DFT/LDA band structure for  $\text{YNiO}_2$  and (b) its magnified figure. The zero energy corresponds to the Fermi level.

we use Y as the cation. The computational conditions for the DFT/LDA and GW are as follows. The calculation is based on the full-potential linear muffin-tin orbital implementation [70]. The exchange correlation functional is obtained by the local density approximation of the Ceperley-Alder type [71]. We neglect the spin-polarization. The self-consistent LDA calculation is done for the  $12 \times 12 \times 12$   $k$ -mesh. The muffintin (MT) radii are as follows:  $R_{\text{Y}}^{\text{MT}} = 2.9$  bohr,  $R_{\text{Ni}}^{\text{MT}} = 2.15$  bohr,  $R_{\text{O}}^{\text{MT}} = 1.5$  bohr, The angular momentum of the atomic orbitals is taken into account up to  $l = 4$  for all the atoms.

The cRPA and GW calculations use a mixed basis consisting of products of two atomic orbitals and interstitial plane waves [72]. In the cRPA and GW calculation, the  $6 \times 6 \times 6$   $k$ -mesh is employed for  $\text{YNiO}_2$ . we interpolate the mesh using the tetrahedron method to treat the screening effect accurately [73, 74]. We disentangle the target band from other bands when the target band crosses another band and construct orthogonalized two separated Hilbert spaces [75]. We include bands about from  $-25$  eV to  $120$  eV for calculation of the screened interaction and the self-energy.

### 3 RESULT

Figure 1 shows the crystal structure of the infinite-layer nickelates. The block layer is a single lanthanide cation and has large interstitial regions surrounded by cations. This is one of the reasons for the formation of electron pockets originating from the block layer, as described below.

Figure 2 shows the band structure of  $\text{YNiO}_2$  in the LDA. The band structure of  $\text{YNiO}_2$  is very similar to that of  $\text{NdNiO}_2$  if we eliminate the Nd  $4f$  bands. The  $3d_{x^2-y^2}$  antibonding state mainly forms the Fermi surface, which is a feature commonly seen in the cuprate superconductors. Reflecting the square

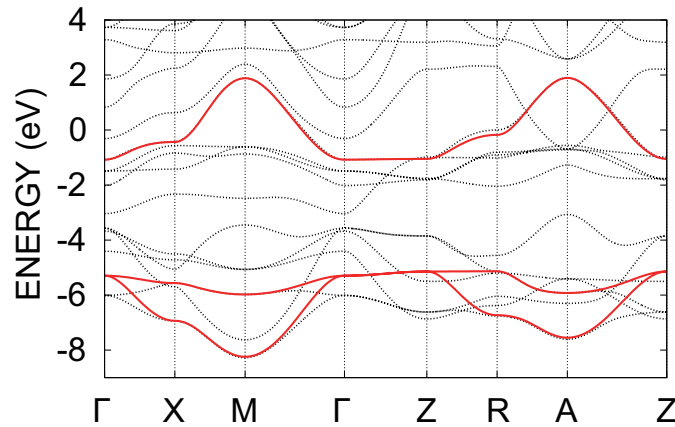


**Figure 3.** Electronic band structure of the three-orbital model in the LDA (solid lines). The zero energy corresponds to the Fermi level. For comparison, the band structures in the LDA is also given (dotted lines).

**Table 1.** Transfer integrals and effective interactions in the three-orbital Hamiltonian for YNiO<sub>2</sub> (in eV). Both the one- and two-body part of the Hamiltonian are constructed based on the LDA band structure.  $v$ ,  $U(0)$ ,  $J_v$ , and  $J(0)$  represent the bare Coulomb, the static values of the effective Coulomb, bare exchange interactions, and exchange interactions, respectively (at  $\omega = 0$ ). The index 'n' and 'nn' represent the nearest unit cell [1,0,0] and the next-nearest unit cell [1,1,0], respectively.

$t(\text{LDA})$	(0, 0, 0)			(1, 0, 0)			(1, 1, 0)			(2, 0, 0)		
	$x^2 - y^2$	$p_1$	$p_2$	$x^2 - y^2$	$p_1$	$p_2$	$x^2 - y^2$	$p_1$	$p_2$	$x^2 - y^2$	$p_1$	$p_2$
$x^2 - y^2$	-1.377	-1.327	1.327	0.062	-0.018	-0.027	0.024	-0.006	0.006	-0.005	0.001	0.000
$p_1$	-1.327	-5.355	-0.671	1.327	0.043	0.671	-0.027	0.037	0.002	0.018	-0.006	0.002
$p_2$	1.327	-0.671	-5.355	-0.027	-0.002	-0.043	0.027	0.002	0.037	0.000	0.000	0.000
	$v$			$U(0)$			$J_v$			$J(0)$		
	$x^2 - y^2$	$p_1$	$p_2$	$x^2 - y^2$	$p_1$	$p_2$	$x^2 - y^2$	$p_1$	$p_2$	$x^2 - y^2$	$p_1$	$p_2$
$x^2 - y^2$	26.406	7.886	7.886	4.599	0.763	0.763		0.116	0.116		0.066	0.066
$p_1$	7.886	17.231	5.278	0.763	4.127	0.499	0.116		0.040	0.066		0.019
$p_2$	7.886	5.278	17.231	0.763	0.499	4.127	0.116	0.040		0.066	0.019	
	$v_n$			$V_n(0)$			$v_{nn}$			$V_{nn}(0)$		
	$x^2 - y^2$	$p_1$	$p_2$	$x^2 - y^2$	$p_1$	$p_2$	$x^2 - y^2$	$p_1$	$p_2$	$x^2 - y^2$	$p_1$	$p_2$
$x^2 - y^2$	3.730	7.886	3.286	0.157	0.763	0.124	2.644	3.286	3.286	0.061	0.124	0.124
$p_1$	2.530	3.841	2.379	0.080	0.250	0.059	2.124	2.643	2.379	0.035	0.086	0.059
$p_2$	3.286	5.278	3.566	0.124	0.499	0.155	2.124	2.379	2.643	0.035	0.059	0.086

planar crystal field of oxygen around the nickel site, the other  $d$  bands are almost fully occupied. However, differently from the cuprates, the infinite-layer nickelates have additional small electron pockets around the  $\Gamma$  and  $A$  points. These electron pockets originate from the  $d$ -orbital and the interstitial state in the block layer, respectively. The energy difference between the  $3d$  bands of Ni<sup>1+</sup> and the  $2p$  bands of O<sup>2-</sup> is larger than that between Cu<sup>2+</sup> and O<sup>2-</sup> in copper oxides, and they are energetically separated near  $-3$  eV.

The interstitial state is located at  $-1.4$  eV at the  $A$  point, and has a band inversion between  $yz/zx$  orbitals around the  $A$  point. Because of the inversion between bands with different numbers of degeneracies, the bands of the interstitial  $s$  and the  $yz/zx$  are continuously connected from the conduction band to the valence band. Since this band inversion is buried in the metallic band, it will be difficult to observe the surface state associated with the band inversion.

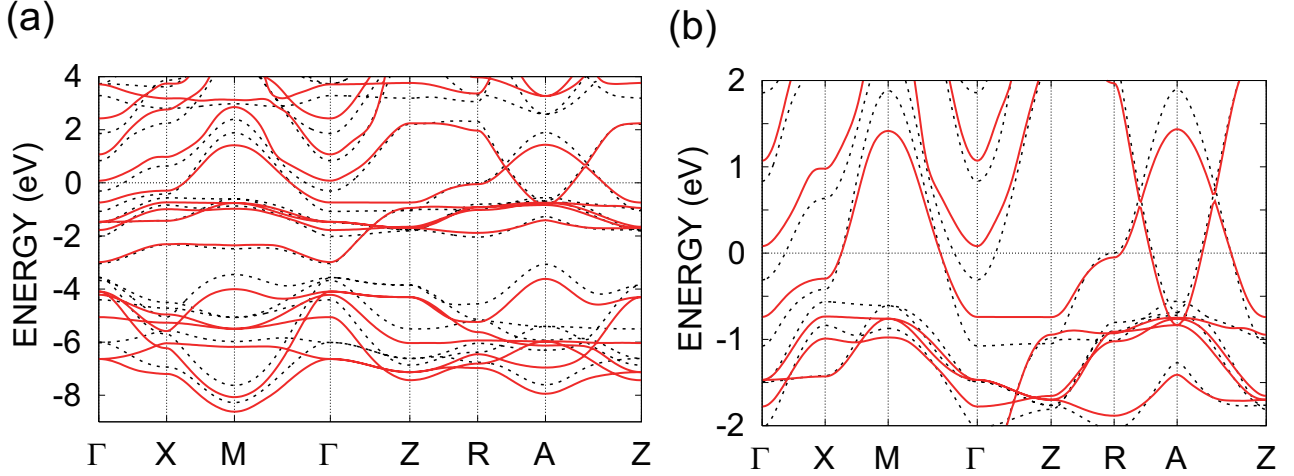


**Figure 4.** (a) GW band structure for  $\text{YNiO}_2$  and (b) its magnified figure (solid lines). For comparison, the band structures in the LDA is also given (dotted lines). The zero energy corresponds to the Fermi level.

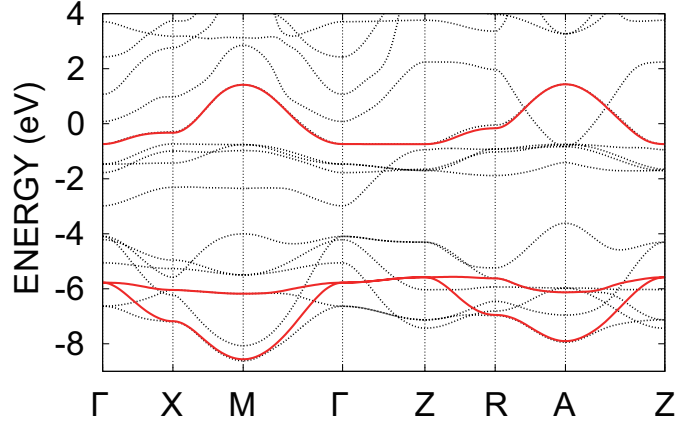


**Figure 5.** Electronic band structure of the three-orbital model in the GWA (solid lines). The zero energy corresponds to the Fermi level. For comparison, the band structures in the GWA is also given (dotted lines).

In this paper, we derive a three-orbital effective model consisting of the Ni  $3d_{x^2-y^2}$  orbital and two O  $2p$  orbitals forming a  $\sigma$ -bonding. We first construct the maximally localized Wannier functions [29, 30] for these orbitals and evaluate the parameters in the tight-binding model (see Table 1). The obtained model has a larger energy difference between the  $3d_{x^2-y^2}$  and  $2p$  orbitals than that of the cuprate, and is closer to the Mott-Hubbard type.

We then calculate the effective interaction for the three-orbital model by the cRPA method. The obtained effective interactions are summarized in Table 1. The bare Coulomb interaction  $v$  is slightly smaller than that of the copper oxides (Ni  $3d_{x^2-y^2}$ :  $\sim 26$  eV, Cu  $d_{x^2-y^2}$ :  $\sim 29$  eV in Refs. [37, 38]), and the dielectric constant  $U/v$  is smaller than that of the copper oxides partially due to the metallic screening from the block layer.

We next show the band structure in the GWA in Fig. 4. In the GWA, the energy difference between the strongly correlated Ni  $3d$  orbitals and the weakly correlated O  $2p$  orbitals is enhanced [33, 76]. Thereby,

**Table 2.** Transfer integrals and effective interactions in the three-band Hamiltonian for YNiO<sub>2</sub> (in eV). The one-body part is obtained from the GW band structure, and the effective interaction is the result of the cRPA calculation for the GW bands.  $v$ ,  $U(0)$ ,  $J_v$ , and  $J(0)$  represent the bare Coulomb, the static values of the effective Coulomb, bare exchange interactions, and exchange interactions, respectively (at  $\omega = 0$ ). The index 'n' and 'nn' represent the nearest unit cell [1,0,0] and the next-nearest unit cell [1,1,0] respectively.

$t(\text{GW})$	(0, 0, 0)			(1, 0, 0)			(1, 1, 0)			(2, 0, 0)		
	$x^2 - y^2$	$p_1$	$p_2$	$x^2 - y^2$	$p_1$	$p_2$	$x^2 - y^2$	$p_1$	$p_2$	$x^2 - y^2$	$p_1$	$p_2$
$x^2 - y^2$	-1.204	-1.288	1.288	0.094	-0.025	-0.021	0.015	-0.005	0.005	-0.002	0.001	0.001
$p_1$	-1.288	-5.802	-0.640	1.288	0.037	0.640	-0.021	0.031	0.007	0.025	-0.004	0.007
$p_2$	1.288	-0.640	-5.802	-0.021	-0.007	-0.022	0.021	0.007	0.031	0.001	0.000	-0.003
	$v$			$U(0)$			$J_v$			$J(0)$		
	$x^2 - y^2$	$p_1$	$p_2$	$x^2 - y^2$	$p_1$	$p_2$	$x^2 - y^2$	$p_1$	$p_2$	$x^2 - y^2$	$p_1$	$p_2$
$x^2 - y^2$	26.596	7.901	7.901	5.019	0.932	0.932		0.114	0.114		0.066	0.066
$p_1$	7.901	17.383	5.280	0.932	4.510	0.624	0.114		0.038	0.066		0.019
$p_2$	7.901	5.280	17.382	0.932	0.624	4.510	0.114	0.038		0.066	0.019	
	$v_n$			$V_n(0)$			$v_{nn}$			$V_{nn}(0)$		
	$x^2 - y^2$	$p_1$	$p_2$	$x^2 - y^2$	$p_1$	$p_2$	$x^2 - y^2$	$p_1$	$p_2$	$x^2 - y^2$	$p_1$	$p_2$
$x^2 - y^2$	3.727	7.901	3.285	0.223	0.932	0.181	2.643	3.285	3.285	0.094	0.181	0.181
$p_1$	2.528	3.840	2.379	0.116	0.332	0.094	2.123	2.641	2.379	0.057	0.130	0.094
$p_2$	3.285	5.280	3.567	0.181	0.624	0.230	2.123	2.379	2.641	0.057	0.094	0.13

the energy gap between the  $d$ - and  $p$ -bands around  $-3$  eV is increased. On the other hand, the bandwidth of the antibonding orbitals of the  $3d_{x^2-y^2}$  orbital decreases. The contribution of the O  $2p$  orbitals to the antibonding orbitals decreases due to the increase in the energy difference between the  $d$ - and  $p$ -orbitals. The bandwidth of the strongly correlated orbitals in the GWA is also reduced compared to that in the LDA due to the effect of the frequency dependence of the self-energy. The bandwidth of the O  $2p$  orbitals remains approximately the same as that in the LDA.

In the GWA, the position of the valence band is lifted up from that in the LDA. In particular, the electron pocket originating from the  $d$  orbital in the block layer near the  $\Gamma$  point disappears. On the other hand, the bottom of the band originating from the interstitial state still creates the electron pocket around the  $A$  point even in the GWA.

We summarize the hopping parameters in Table 2. The difference in the on-site potential between the  $3d_{x^2-y^2}$  and  $2p$  orbitals increase from 3.98 eV to 4.60 eV. The nearest-neighbor hopping between the  $3d_{x^2-y^2}$  and  $2p$  orbitals is almost the same ( $\sim -1.3$  eV), but slightly reduced due to the renormalization factor in the GWA. The increase of the onsite potential difference between the atomic  $3d_{x^2-y^2}$  and  $2p$  orbitals results in an decrease of the oxygen contribution to the antibonding  $3d_{x^2-y^2}$  orbitals and decrease of the hopping between the antibonding  $3d_{x^2-y^2}$  orbitals.

The screening effect of the system is reduced compared to that in the LDA mainly due to the increase of the charge-transfer energy, which increases the bare Coulomb interaction of the  $3d_{x^2-y^2}$  band and reduces the screening effect from the  $2p$  bands. The bands originating from the block layer as well as the O  $2p$  orbitals in the GWA move away from the Fermi level compared to the LDA, which makes the screening effect weaker. The disappearance of the metallic screening from the electron pocket at the  $\Gamma$  point also partially contribute to the reduction of the correlation. Therefore, the value of the effective interaction is increased from that in the LDA. For example, while the on-site interaction is 4.6 eV for the  $3d_{x^2-y^2}$  orbital and 4.1 eV for the  $2p$  orbital in the LDA-based cRPA calculation, the GWA-based cRPA gives 5.0

**Table 3.** Transfer integral and effective interaction in the one-band Hamiltonian for YNiO<sub>2</sub> (in eV). Both the one-body and two-body parts in the Hamiltonian are derived based on the LDA band structure.  $v$  and  $U(0)$  represent the bare Coulomb interaction and the static value of the effective Coulomb interaction, respectively (at  $\omega = 0$ ). The index 'n' and 'nn' represent the nearest unit cell [1,0,0] and the next-nearest unit cell [1,1,0], respectively.

$t(\text{LDA})$	(0, 0, 0)	(1, 0, 0)	(1, 1, 0)	(2, 0, 0)	$U/v$	$ U/t $
$x^2 - y^2$	0.211	-0.357	0.093	-0.046	0.149	8.15
	$v$	$U(0)$	$v_n$	$V_n(0)$	$v_{nn}$	$V_{nn}(0)$
$x^2 - y^2$	19.578	2.910	3.981	0.229	2.685	0.091

eV for the  $3d_{x^2-y^2}$  orbital and 4.5 eV for the  $2p$  orbital. The nearest-neighbor interactions also increase from 0.16 eV to 0.22 eV for the  $3d_{x^2-y^2}$  orbital. Note that the metallic screening from the electron pocket near the A point still remains even in the GWA.<sup>3</sup>

## 4 CONCLUSION

We derived a three-orbital low-energy model for the infinite-layer nickelates based on the GWA. In the GWA, the O  $2p$  bands locate deeper below the Fermi level, and the bandwidth of the Ni  $3d_{x^2-y^2}$  band is narrower than that in the LDA calculation. Due to the isolation of the low-energy Ni  $3d_{x^2-y^2}$  band, the screening effect becomes less effective, leading to larger interaction parameters in the Hamiltonian. Thus the GW-based *ab initio* downfolding gives a more correlated model than the LDA-based downfolding.

## APPENDIX

For reference, we summarize the parameters in the single-orbital model in Tables 3 and 4. Special attention should be paid to the strength of the interaction in the GWA-based effective single-orbital model (see Ref. [38]). In the copper oxides, the correlation effect beyond the RPA between the  $d$  and  $p$  orbitals in the three-orbital model is not small. Therefore, in order to calculate the single-orbital model accurately, it is necessary to treat the screening effect originating from the bonding and nonbonding bands beyond the RPA. To do so, we need to solve the three-orbital model once with a low-energy solver such as the VMC and estimate the energy corrections between the  $d$  and  $p$  orbitals beyond the GWA. By combining such a correction with the GW self-energy correction, we can calculate the band structure beyond the GWA, and can estimate a single-orbital model with high accuracy (See Ref. [38] for details of the method). Because the nickelates have a qualitatively similar band structure to the cuprates, the reliability of the GWA-based single-orbital model for the nickelates also needs to be carefully examined: in particular, the correlation strength  $|U/t|$  might be overestimated.

## CONFLICT OF INTEREST STATEMENT

The authors declare that the research was conducted in the absence of any commercial or financial relationships that could be construed as a potential conflict of interest.

## AUTHOR CONTRIBUTIONS

MH conducted calculations. All authors contributed to writing the article.

<sup>3</sup> We note that there is a proposal that the electron pocket at the A point can be eliminated by designing a different type of the block layer [33].



**Table 4.** Transfer integral and effective interaction in the one-band Hamiltonian for YNiO<sub>2</sub> (in eV). The one-body part is derived based on the GW band structure, and the effective interaction is the result of the cRPA calculation for the GW bands.  $v$  and  $U(0)$  represent the bare Coulomb interaction and the static value of the effective Coulomb interaction, respectively (at  $\omega = 0$ ). The index 'n' and 'nn' represent the nearest unit cell [1,0,0] and the next-nearest unit cell [1,1,0] respectively.

$t(\text{GW})$	(0, 0, 0)	(1, 0, 0)	(1, 1, 0)	(2, 0, 0)	$U/v$	$ U/t $
$x^2 - y^2$	0.172	-0.271	0.075	-0.033	0.167	12.94
	$v$	$U(0)$	$v_n$	$V_n(0)$	$v_{nn}$	$V_{nn}(0)$
$x^2 - y^2$	20.948	3.508	3.957	0.300	2.677	0.131

## FUNDING

We acknowledge funding through Grant-in-Aids for Scientific Research (JSPS KAKENHI) [Grant No. 20K14423 (YN), 21H01041 (YN), and 19H05825 (RA)] and “Program for Promoting Researches on the Supercomputer Fugaku” (Basic Science for Emergence and Functionality in Quantum Matter — Innovative Strongly-Correlated Electron Science by Integration of “Fugaku” and Frontier Experiments—) (Grant No. JPMXP1020200104) from MEXT.

## ACKNOWLEDGMENTS

We thank Terumasa Tadano and Motoharu Kitatani for valuable discussions.

## REFERENCES

- [1] Li D, Lee K, Wang BY, Osada M, Crossley S, Lee HR, et al. Superconductivity in an infinite-layer nickelate. *Nature* **572** (2019) 624–627.
- [2] Norman MR. Entering the Nickel Age of Superconductivity. *Physics* **13** (2020) 85.
- [3] Pickett WE. The dawn of the nickel age of superconductivity. *Nature Reviews Physics* **3** (2021) 7–8.
- [4] Zhang J, Tao X. Review on quasi-2D square planar nickelates. *CrystEngComm* **23** (2021) 3249–3264.
- [5] Botana AS, Bernardini F, Cano A. Nickelate Superconductors: An Ongoing Dialog between Theory and Experiments. *Journal of Experimental and Theoretical Physics* **132** (2021) 618–627.
- [6] Nomura Y, Arita R. Superconductivity in infinite-layer nickelates (2021) arXiv:2107.12923.
- [7] Gu Q, Wen HH. Superconductivity in nickel based 112 systems (2021) arXiv:2109.07654.
- [8] Zeng S, Tang CS, Yin X, Li C, Li M, Huang Z, et al. Phase Diagram and Superconducting Dome of Infinite-Layer Nd<sub>1-x</sub>Sr<sub>x</sub>NiO<sub>2</sub> Thin Films. *Phys. Rev. Lett.* **125** (2020) 147003. doi:10.1103/PhysRevLett.125.147003.
- [9] Gu Q, Li Y, Wan S, Li H, Guo W, Yang H, et al. Single particle tunneling spectrum of superconducting Nd<sub>1-x</sub>Sr<sub>x</sub>NiO<sub>2</sub> thin films. *Nat. Commun.* **11** (2020) 6027.
- [10] Gao Q, Zhao Y, Zhou XJ, Zhu Z. Preparation of Superconducting Thin Films of Infinite-Layer Nickelate Nd<sub>0.8</sub>Sr<sub>0.2</sub>NiO<sub>2</sub>. *Chinese Physics Letters* **38** (2021) 077401. doi:10.1088/0256-307X/38/7/077401.
- [11] Zhou XR, Feng ZX, Qin PX, Yan H, Wang XN, Nie P, et al. Negligible oxygen vacancies, low critical current density, electric-field modulation, in-plane anisotropic and high-field transport of a superconducting Nd<sub>0.8</sub>Sr<sub>0.2</sub>NiO<sub>2</sub>/SrTiO<sub>3</sub> heterostructure. *Rare Metals* (2021).
- [12] Li Y, Sun W, Yang J, Cai X, Guo W, Gu Z, et al. Impact of cation stoichiometry on the crystalline structure and superconductivity in nickelates. *Frontiers in Physics* **9** (2021) 443. doi:10.3389/fphy.2021.719534.

- [13] Osada M, Wang BY, Goodge BH, Lee K, Yoon H, Sakuma K, et al. A Superconducting Praseodymium Nickelate with Infinite Layer Structure. *Nano Letters* **20** (2020) 5735–5740.
- [14] Osada M, Wang BY, Lee K, Li D, Hwang HY. Phase diagram of infinite layer praseodymium nickelate  $\text{Pr}_{1-x}\text{Sr}_x\text{NiO}_2$  thin films. *Phys. Rev. Materials* **4** (2020) 121801. doi:10.1103/PhysRevMaterials.4.121801.
- [15] Osada M, Wang BY, Goodge BH, Harvey SP, Lee K, Li D, et al. Nickelate superconductivity without rare-earth magnetism:  $(\text{La,Sr})\text{NiO}_2$ . *Adv. Mater.* (2021) 2104083.
- [16] Zeng SW, Li CJ, Chow LE, Cao Y, Zhang ZT, Tang CS, et al. Superconductivity in infinite-layer lanthanide nickelates (2021) arXiv:2105.13492.
- [17] Pan GA, Ferenc Segedin D, LaBollita H, Song Q, Nica EM, Goodge BH, et al. Superconductivity in a quintuple-layer square-planar nickelate. *Nature Materials* (2021).
- [18] Nomura Y, Hirayama M, Tadano T, Yoshimoto Y, Nakamura K, Arita R. Formation of a two-dimensional single-component correlated electron system and band engineering in the nickelate superconductor  $\text{NdNiO}_2$ . *Phys. Rev. B* **100** (2019) 205138. doi:10.1103/PhysRevB.100.205138.
- [19] Adhikary P, Bandyopadhyay S, Das T, Dasgupta I, Saha-Dasgupta T. Orbital-selective superconductivity in a two-band model of infinite-layer nickelates. *Phys. Rev. B* **102** (2020) 100501. doi:10.1103/PhysRevB.102.100501.
- [20] Wang Z, Zhang GM, Yang Yf, Zhang FC. Distinct pairing symmetries of superconductivity in infinite-layer nickelates. *Phys. Rev. B* **102** (2020) 220501. doi:10.1103/PhysRevB.102.220501.
- [21] Kitamine N, Ochi M, Kuroki K. Designing nickelate superconductors with  $d^8$  configuration exploiting mixed-anion strategy. *Phys. Rev. Research* **2** (2020) 042032. doi:10.1103/PhysRevResearch.2.042032.
- [22] Wu X, Jiang K, Sante DD, Hanke W, Schnyder AP, Hu J, et al. Surface  $s$ -wave superconductivity for oxide-terminated infinite-layer nickelates (2020) arXiv:2008.06009.
- [23] Choubey P, Eremin IM. Electronic theory for scanning tunneling microscopy spectra in infinite-layer nickelate superconductors. *Phys. Rev. B* **104** (2021) 144504. doi:10.1103/PhysRevB.104.144504.
- [24] Sakakibara H, Usui H, Suzuki K, Kotani T, Aoki H, Kuroki K. Model Construction and a Possibility of Cupratelike Pairing in a New  $d^9$  Nickelate Superconductor  $(\text{Nd,Sr})\text{NiO}_2$ . *Phys. Rev. Lett.* **125** (2020) 077003. doi:10.1103/PhysRevLett.125.077003.
- [25] Hirsch J, Marsiglio F. Hole superconductivity in infinite-layer nickelates. *Physica C: Superconductivity and its Applications* **566** (2019) 1353534. doi:https://doi.org/10.1016/j.physc.2019.1353534.
- [26] Wu X, Di Sante D, Schwemmer T, Hanke W, Hwang HY, Raghu S, et al. Robust  $d_{x^2-y^2}$ -wave superconductivity of infinite-layer nickelates. *Phys. Rev. B* **101** (2020) 060504. doi:10.1103/PhysRevB.101.060504.
- [27] Giustino F. Electron-phonon interactions from first principles. *Rev. Mod. Phys.* **89** (2017) 015003. doi:10.1103/RevModPhys.89.015003.
- [28] Flores-Livas JA, Boeri L, Sanna A, Profeta G, Arita R, Eremets M. A perspective on conventional high-temperature superconductors at high pressure: Methods and materials. *Physics Reports* **856** (2020) 1–78. doi:https://doi.org/10.1016/j.physrep.2020.02.003. A perspective on conventional high-temperature superconductors at high pressure: Methods and materials.
- [29] Marzari N, Vanderbilt D. Maximally localized generalized Wannier functions for composite energy bands. *Phys. Rev. B* **56** (1997) 12847–12865. doi:10.1103/PhysRevB.56.12847.
- [30] Souza I, Marzari N, Vanderbilt D. Maximally localized Wannier functions for entangled energy bands. *Phys. Rev. B* **65** (2001) 035109. doi:10.1103/PhysRevB.65.035109.

- [31] Aryasetiawan F, Imada M, Georges A, Kotliar G, Biermann S, Lichtenstein AI. Frequency-dependent local interactions and low-energy effective models from electronic structure calculations. *Phys. Rev. B* **70** (2004) 195104. doi:10.1103/PhysRevB.70.195104.
- [32] Imada M, Miyake T. Electronic structure calculation by first principles for strongly correlated electron systems. *J. Phys. Soc. Jpn.* **79** (2010) 2001.
- [33] Hirayama M, Tadano T, Nomura Y, Arita R. Materials design of dynamically stable  $d^9$  layered nickelates. *Phys. Rev. B* **101** (2020) 075107. doi:10.1103/PhysRevB.101.075107.
- [34] Nomura Y, Nomoto T, Hirayama M, Arita R. Magnetic exchange coupling in cuprate-analog  $d^9$  nickelates. *Phys. Rev. Research* **2** (2020) 043144. doi:10.1103/PhysRevResearch.2.043144.
- [35] Hirayama M, Miyake T, Imada M, Biermann S. Low-energy effective hamiltonians for correlated electron systems beyond density functional theory. *Phys. Rev. B* **96** (2017) 075102.
- [36] Hirayama M, Miyake T, Imada M. Derivation of static low-energy effective models by an ab initio downfolding method without double counting of coulomb correlations: Application to  $\text{SrVO}_3$ ,  $\text{FeSe}$ , and  $\text{FeTe}$ . *Phys. Rev. B* **87** (2013) 195144. doi:10.1103/PhysRevB.87.195144.
- [37] Hirayama M, Yamaji Y, Misawa T, Imada M. Ab initio effective Hamiltonians for cuprate superconductors. *Phys. Rev. B* **98** (2018) 134501. doi:10.1103/PhysRevB.98.134501.
- [38] Hirayama M, Misawa T, Ohgoe T, Yamaji Y, Imada M. Effective Hamiltonian for cuprate superconductors derived from multiscale ab initio scheme with level renormalization. *Phys. Rev. B* **99** (2019) 245155. doi:10.1103/PhysRevB.99.245155.
- [39] Ohgoe T, Hirayama M, Misawa T, Ido K, Yamaji Y, Imada M. Ab initio study of superconductivity and inhomogeneity in a hg-based cuprate superconductor. *Phys. Rev. B* **101** (2020) 045124. doi:10.1103/PhysRevB.101.045124.
- [40] Jiang M, Berciu M, Sawatzky GA. Critical Nature of the Ni Spin State in Doped  $\text{NdNiO}_2$ . *Phys. Rev. Lett.* **124** (2020) 207004. doi:10.1103/PhysRevLett.124.207004.
- [41] Zhang YH, Vishwanath A. Type-II  $t$ - $J$  model in superconducting nickelate  $\text{Nd}_{1-x}\text{Sr}_x\text{NiO}_2$ . *Phys. Rev. Research* **2** (2020) 023112. doi:10.1103/PhysRevResearch.2.023112.
- [42] Werner P, Hoshino S. Nickelate superconductors: Multiorbital nature and spin freezing. *Phys. Rev. B* **101** (2020) 041104. doi:10.1103/PhysRevB.101.041104.
- [43] Petocchi F, Christiansson V, Nilsson F, Aryasetiawan F, Werner P. Normal State of  $\text{Nd}_{1-x}\text{Sr}_x\text{NiO}_2$  from Self-Consistent  $GW$  + EDMFT. *Phys. Rev. X* **10** (2020) 041047. doi:10.1103/PhysRevX.10.041047.
- [44] Hu LH, Wu C. Two-band model for magnetism and superconductivity in nickelates. *Phys. Rev. Research* **1** (2019) 032046. doi:10.1103/PhysRevResearch.1.032046.
- [45] Lechermann F. Late transition metal oxides with infinite-layer structure: Nickelates versus cuprates. *Phys. Rev. B* **101** (2020) 081110. doi:10.1103/PhysRevB.101.081110.
- [46] Lechermann F. Multiorbital Processes Rule the  $\text{Nd}_{1-x}\text{Sr}_x\text{NiO}_2$  Normal State. *Phys. Rev. X* **10** (2020) 041002. doi:10.1103/PhysRevX.10.041002.
- [47] Lechermann F. Doping-dependent character and possible magnetic ordering of  $\text{NdNiO}_2$ . *Phys. Rev. Materials* **5** (2021) 044803. doi:10.1103/PhysRevMaterials.5.044803.
- [48] Chang J, Zhao J, Ding Y. Hund-Heisenberg model in superconducting infinite-layer nickelates. *The European Physical Journal B* **93** (2020) 220.
- [49] Wang Y, Kang CJ, Miao H, Kotliar G. Hund's metal physics: From  $\text{SrNiO}_2$  to  $\text{LaNiO}_2$ . *Phys. Rev. B* **102** (2020) 161118. doi:10.1103/PhysRevB.102.161118.
- [50] Liu Z, Xu C, Cao C, Zhu W, Wang ZF, Yang J. Doping dependence of electronic structure of infinite-layer  $\text{NdNiO}_2$ . *Phys. Rev. B* **103** (2021) 045103. doi:10.1103/PhysRevB.103.045103.

- [51] Kang B, Melnick C, Semon P, Ryee S, Han MJ, Kotliar G, et al. Infinite-layer nickelates as Ni- $e_g$  Hund's metals (2021) arXiv:2007.14610.
- [52] Choi MY, Pickett WE, Lee KW. Fluctuation-frustrated flat band instabilities in NdNiO<sub>2</sub>. *Phys. Rev. Research* **2** (2020) 033445. doi:10.1103/PhysRevResearch.2.033445.
- [53] Jiang P, Si L, Liao Z, Zhong Z. Electronic structure of rare-earth infinite-layer RNiO<sub>2</sub> ( $R = \text{La, Nd}$ ). *Phys. Rev. B* **100** (2019) 201106. doi:10.1103/PhysRevB.100.201106.
- [54] Choi MY, Lee KW, Pickett WE. Role of 4*f* states in infinite-layer NdNiO<sub>2</sub>. *Phys. Rev. B* **101** (2020) 020503. doi:10.1103/PhysRevB.101.020503.
- [55] Zhang R, Lane C, Singh B, Nokelainen J, Barbiellini B, Markiewicz RS, et al. Magnetic and *f*-electron effects in LaNiO<sub>2</sub> and NdNiO<sub>2</sub> nickelates with cuprate-like  $3d_{x^2-y^2}$  band. *Communications Physics* **4** (2021) 118.
- [56] Bandyopadhyay S, Adhikary P, Das T, Dasgupta I, Saha-Dasgupta T. Superconductivity in infinite-layer nickelates: Role of *f* orbitals. *Phys. Rev. B* **102** (2020) 220502. doi:10.1103/PhysRevB.102.220502.
- [57] Hepting M, Li D, Jia CJ, Lu H, Paris E, Tseng Y, et al. Electronic structure of the parent compound of superconducting infinite-layer nickelates. *Nature Materials* **19** (2020) 381–385.
- [58] Zhang GM, Yang YF, Zhang FC. Self-doped Mott insulator for parent compounds of nickelate superconductors. *Phys. Rev. B* **101** (2020) 020501. doi:10.1103/PhysRevB.101.020501.
- [59] Gu Y, Zhu S, Wang X, Hu J, Chen H. A substantial hybridization between correlated Ni-*d* orbital and itinerant electrons in infinite-layer nickelates. *Communications Physics* **3** (2020) 84.
- [60] Fu Y, Wang L, Cheng H, Pei S, Zhou X, Chen J, et al. Core-level x-ray photoemission and Raman spectroscopy studies on electronic structures in Mott-Hubbard type nickelate oxide NdNiO<sub>2</sub> (2019) arXiv:1911.03177.
- [61] Goodge BH, Li D, Lee K, Osada M, Wang BY, Sawatzky GA, et al. Doping evolution of the Mott–Hubbard landscape in infinite-layer nickelates. *Proceedings of the National Academy of Sciences* **118** (2021).
- [62] Kitatani M, Si L, Janson O, Arita R, Zhong Z, Held K. Nickelate superconductors—a renaissance of the one-band Hubbard model. *npj Quantum Materials* **5** (2020) 59.
- [63] Karp J, Hampel A, Zingl M, Botana AS, Park H, Norman MR, et al. Comparative many-body study of Pr<sub>4</sub>Ni<sub>3</sub>O<sub>8</sub> and NdNiO<sub>2</sub>. *Phys. Rev. B* **102** (2020) 245130. doi:10.1103/PhysRevB.102.245130.
- [64] Higashi K, Winder M, Kuneš J, Hariki A. Core-level x-ray spectroscopy of infinite-layer nickelate: LDA + DMFT study. *Phys. Rev. X* **11** (2021) 041009. doi:10.1103/PhysRevX.11.041009.
- [65] Karp J, Botana AS, Norman MR, Park H, Zingl M, Millis A. Many-Body Electronic Structure of NdNiO<sub>2</sub> and CaCuO<sub>2</sub>. *Phys. Rev. X* **10** (2020) 021061. doi:10.1103/PhysRevX.10.021061.
- [66] Lang ZJ, Jiang R, Ku W. Strongly correlated doped hole carriers in the superconducting nickelates: Their location, local many-body state, and low-energy effective Hamiltonian. *Phys. Rev. B* **103** (2021) L180502. doi:10.1103/PhysRevB.103.L180502.
- [67] Worm P, Si L, Kitatani M, Arita R, Tomczak JM, Held K. Correlations turn electronic structure of finite-layer nickelates upside down (2021) arXiv:2111.12697.
- [68] Zaanen J, Sawatzky GA, Allen JW. Band gaps and electronic structure of transition-metal compounds. *Phys. Rev. Lett.* **55** (1985) 418–421. doi:10.1103/PhysRevLett.55.418.
- [69] Crespin M, Isnard O, Dubois F, Choisnet J, Odier P. Lanio2: Synthesis and structural characterization. *Journal of Solid State Chemistry* **178** (2005) 1326–1334. doi:https://doi.org/10.1016/j.jssc.2005.01.023.

- 
- [70] Methfessel M, van Schilfgaarde M, Casali RA. in *Lecture Notes in Physics, Vol. 535*, edited by H. Dreysse (Springer-Verlag, Berlin) (2000).
- [71] Ceperley DM, Alder BJ. Ground state of the electron gas by a stochastic method. *Phys. Rev. Lett.* **45** (1980) 566–569. doi:10.1103/PhysRevLett.45.566.
- [72] van Schilfgaarde M, Kotani T, Faleev SV. *Phys. Rev. B* **74** (2006) 245125.
- [73] Fujiwara T, Yamamoto S, Ishii Y. *J. Phys. Soc. Jpn.* **72** (2003) 777.
- [74] Nohara Y, Yamamoto S, Fujiwara T. *Phys. Rev. B* **79** (2009) 195110.
- [75] Miyake T, Aryasetiawan F, Imada M. *Phys. Rev. B* **80** (2009) 155134.
- [76] Olevano V, Bernardini F, Blase X, Cano A. Ab initio many-body *gw* correlations in the electronic structure of  $\text{LaNiO}_2$ . *Phys. Rev. B* **101** (2020) 161102. doi:10.1103/PhysRevB.101.161102.